Clinical & Experimental Metastasis **20:** 121–133, 2003.

Establishment of red fluorescent protein-tagged HeLa tumor metastasis models: Determination of DsRed2 insertion effects and comparison of metastatic patterns after subcutaneous, intraperitoneal, or intravenous injection

Jau-Yeong Lu[1], Hui-Chun Chen[2], Ricky Yuan-Yuan Chu[3], Tsu-Chun Emma Lin[3], Ping-I Hsu[1], Ming-Shyan Huang[4], Ching-Jiunn Tseng[3] & Michael Hsiao[3]

[1]*Department of Internal Medicine, Kaohsiung Veterans General Hospital, Kaohsiung, Taiwan;* [2]*Department of Radiation Oncology, Kaohsiung Chang-Gung Memorial Hospital, Kaohsiung, Taiwan;* [3]*Department of Medical Education and Research, Kaohsiung Veterans General Hospital, Kaohsiung, Taiwan;* [4]*Department of Internal Medicine, Kaohsiung Medical University, Kaohsiung, Taiwan*

Received 12 August 2002; accepted in revised form 1 October 2002

Key words: Cervical carcinoma, DsRed2, metastasis model, SCID mice

Abstract

Metastasis is the leading cause of death in patients with cervical cancer. In this report, we establish novel fluorescent HeLa tumor metastasis models to determine whether HeLa transfected with the enhanced red fluorescent protein (DsRed2) gene *in vitro* and xenotransplanted through subcutaneous, intraperitoneal, or intravenous route into SCID mice would permit the detection of tumor micro-metastasis *in vivo*. Our results showed that DsRed2 insertions did not interfere the tumorigenic properties of HeLa cells. We also demonstrated that DsRed2-transduced HeLa cells maintained stable high-level DsRed2 expressions during their growth *in vivo*. DsRed2 fluorescence clearly demarcated the primary seeding place and readily allowed for the visualization of distant micro-metastasis and local invasion at the single-cell level. Lung metastasis, the major cause of cervical carcinoma related death, was found in all three models. However, intravenous injections of the HeLa-DsRed2 cells established tumor foci in the lung, while subcutaneous and intraperitoneal injections only established lung metastasis at single-cell levels. The DsRed2 tagged HeLa cancer model allowed detection and investigation of physiologically relevant patterns of cancer invasion and metastasis *in vivo*.

Introduction

Carcinoma of the cervix is the second leading cause of cancer death in women worldwide and remains a leading cause of mortality among women of reproductive age in developing countries. An estimated 500,000 new cases are diagnosed worldwide each year [1]. Cervical carcinoma arises in women infected with HPV3 and progresses through a multistage process of carcinogenesis [2]. One of the leading causes of cervical cancer death is metastasis. The lung, brain, liver, ovary, and peritoneum are the most common sites for cervical cancer metastasis [3–11]. However, the biology of metastasis in these organs is poorly understood due to the lack of a good animal model. The cellular and molecular changes associated with cancer in animal models for human neoplastic disease are potential keys to understanding disease mechanisms. Several cervical carcinoma animal models have been established [12–14]. However, the early stages of tumor progression and micro-metastasis formation have been difficult to analyze because of the inability to identify small numbers of tumor cells against the background of the host tissue.

Reporter genes such as β-galactosidase, chloramphenicol acetyltransferase and luciferase have played major roles in understanding the molecular mechanisms of gene expression in cultured cells and in transgenic animals. Reporter genes have also been critically important in designing and characterizing delivery systems for gene transfer into somatic tissues in animals. However, measurement of these reporter genes in living animals requires invasive tissue sampling; either biopsy or death. Green fluorescent protein (GFP), produced from the jellyfish Aequorea Victoria, allows direct visualization of proteins in living cells without the need for harsh fixation methods, which can be plaqued by artifacts. It has been used for repetitive, non-invasive reporter-gene imaging in living cultured cells, single cell organisms and multi-cellular organisms transparent to light [15, 16]. The introduction of the green fluorescent protein (GFP) has had a major impact on the field of tumor cell biology. It has enabled the dynamics of a wide variety of tumor cells to be analyzed for such tumor behaviors as growth, invasion, and metastasis, which could not otherwise be easily detected and monitored *in vivo* [17–20].

Correspondence to: Michael Hsiao, Department of Medical Education and Research, Kaohsiung Veterans General Hospital, 386 Ta-Chung 1st Rd, Kaohsiung 813, Taiwan.
Fax: +886-7-3468056; E-mail: mhsiao@isca.vghks.gov.tw

Recently, a red fluorescent protein gene with homology to GFP (drFP583) was cloned from *Discosoma* coral [21], and a humanized version of drFP583, called DsRed, is now commercially available. Even though DsRed shares only 30% amino-acid similarity with GFP, the two crucial residues (tyrosine-66 and glycine-67) that contribute to the chromophore of GFP are conserved. DsRed has an emission maximum of 583 nm. Fully matured DsRed, excited at its 558-nm absorbance maximum, emits a brilliant red light that is similar to rhodamine dyes in terms of wavelength and brightness [22, 23]. Two orthotopic tumor models expressing red fluorescent protein have been recently established [24, 25].

In this study, we used the newly available DsRed2 variant to establish a red fluorescent protein gene that can be included in HeLa cervical cancer metastasis models using SCID mice. We also determined the DsRed2 insertion effects in HeLa cells and the patterns of tumor metastasis after subcutaneous, intraperitoneal, or intravenous injection of DsRed2-HeLa cells.

Materials and methods

DsRed2 expression vector constructions

The pDsRed2-C1 vector containing the enhanced red fluorescent protein gene was purchased from CLONTECH (Clontech, Palo Alto, California, USA). To construct the DsRed2-containing pCI-Neo vector, pDsRed2-C1 was digested with EcoRI and NotI. The pCI-Neo vector was digested with EcoRI and NotI. The DsRed2 cDNA fragment was then unidirectionally subcloned into pCI-Neo. The resulting pCIDsRed2-Neo vector was used to transfect a cervical cancer cell line. The same strategy was also used to generate pCIEGFP-Neo vector from pEGFP-C1.

Cell culture, transfection, and stable clone establishment

The human cervical-cancer cell line HeLa was obtained from ATCC. HeLa cells were cultured in DMEM (GIBCO) supplemented with 10% bovine calf serum (HyClone, Logan, Utah, USA), 2 mM L-glutamine, 100 units/ml penicillin, and 100 μg/ml streptomycin. H1299 cells were incubated in a humidified incubator at 37 °C with 5% CO_2. For transfection, the medium was removed, 70% confluent HeLa cells in 100-mm culture dishes were washed two times with HEPES buffer. Thereafter, HeLa cells were incubated with a mixture of liposome transfection reagent (10 μg pCIDsRed2-Neo, pCIEGFP-Neo, or pCI-Neo plasmid DNA in 1.5 ml HEPES buffer + 100 nM DOTAP/Cholesterol liposome in 1.5 ml Hepes buffer) for 4 h before being replenished with fresh medium. Forty-eight hours after transfection, Hela cells were examined by fluorescence microscopy for the presence of DsRed2 or EGFP positive cells. For selection of DsRed2, EGFP, or vector control transductants, cells were cultured in a selective medium containing 800 μg/ml of G418 for 7 days or until the mock transfected cells died. DsRed2 or EGFP gene-expressed cells were maintained in the selection medium containing 200 μg/ml of G418. Clones expressing EGFP (H1299-EGFP) were isolated with cloning cylinders (Bel-Art Products, Pequannoch, New Jersey, USA) by trypsin/EDTA, and were transferred and amplified by conventional culturing methods. A total of 10 high DsRed2-expressing clones were selected and expanded. These clones were pooled and used to establish *in vivo* tumors in SCID mice.

In vitro *and* in vivo *growth curves*

HeLa, HeLa-VC, HeLa-DsRed2, or HeLa-EGFP cells were seeded at 1×10^5 cell in 12-well plates in triplicates. The cells were harvested and counted every 24 h for a total of 5 days, after which the *in vitro* growth curves were determined. To determine the *in vivo* growth potentials, HeLa, HeLa-VC, HeLa-DsRed2, or HeLa-EGFP cells were grown without G418 for 48 h. Thereafter, 2×10^6 cells were injected into the flanks of SCID mice. Six mice containing six injections of each HeLa, HeLa-VC, HeLa-DsRed2, or HeLa-EGFP cells were selected. Tumor volume was measured every week until death. Standard deviations and statistics were calculated to generate *in vitro* and *in vivo* growth curves.

Colony forming assay

HeLa, HeLa-VC, HeLa-DsRed2, or HeLa-EGFP cells were seeded at 5×10^2 cells in 10-cm plates in triplicates. Cells were allowed to grow in medium without G418 for two weeks. The colonies were washed with PBS, stained with 0.75% crystal violet in methanol for 30 min, and then counted. The data was generated from triplicate experiments.

Establishment of HeLa-DsRed2 metatstasis in SCID mice

SCID mice were anesthetized with an intramuscular injection containing a cocktail of ketamine, 22–44 mg/kg, xylazine, 2.5 mg/kg, and acepromazine, 0.75 mg/kg [26]. 5×10^6 HeLa-DsRed2 cells were diluted in 0.1 ml of PBS and injected into SCID mice through subcutaneous, intraperitoneal, or intravenous routes to establish tumor metastasis.

Optical image analysis of DsRed2-HeLa tumor metastasis

After tumors were established in SCID mice, the performance status of the mice began to decrease. The animals were sacrificed and subjected to fluorescent microscopy examinations when clinical symptoms of terminal illness appeared. The fresh tumors and all major organs were examined for the presence of fluorescence directly under a Zeiss inverted fluorescent microscope equipped with a 100 W mercury lamp power supply, Red fluorescence filter sets (Chroma Technology, Brattleboro, Vermont, USA), and NIKON CoolScan 95 digital camera. Images were captured at the resolution of 1600 × 1200 pixels and transferred directly to a PC for analysis. In addition, the time of death

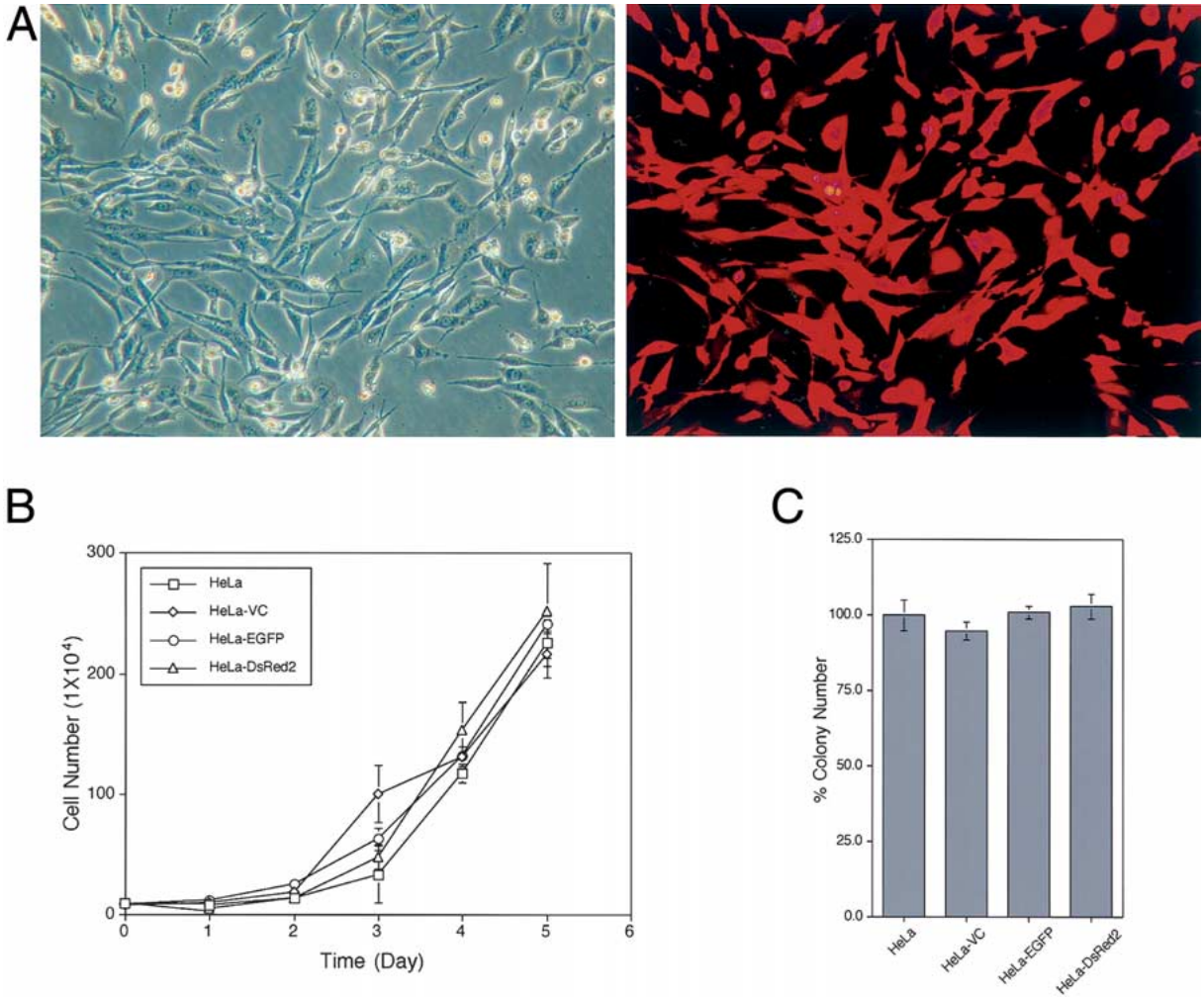

Figure 1. DsRed2 gene expressions in HeLa cells, *in vitro* growth curves, and colony forming assay. Human cervical-cancer cell line HeLa was transfected with pCIDsRed2-Neo expression vector, which expresses DsRed2 and the neomycin resistance genes. Stable, high-expression clones were selected in 800 μg/ml G418. (A) left. daylight picture of HeLa-DsRed2 cells (200×); right. HeLa-DsRed2 picture under fluorescent microscope with rhodamine filter (200×). Note all cells express uniform and strong red fluorescence. (B) *In vitro* tumor growth curves of HeLa-DsRed2 cells and controls. 5×10^4 cells were plated in 6 cm culture dish in triplicates to determine *in vitro* growth curves. Note no statistical differences were found in HeLa, HeLa-VC, HeLa-EGFP, and HeLa-DsRed2 cells. (C) Colony forming assay of HeLa-DsRed2 cells and controls. 500 cells were plated in 10 cm plate in triplicates. Cells were allowed to grow without G418 selection until colony appeared. Total colony numbers were calculated. Colonies generated by Hela cells were calculated as 100%. Note no statistical differences were found in HeLa, HeLa-VC, HeLa-EGFP, and HeLa-DsRed2 cells.

of the animals was also calculated to determine the survival curves.

Histopathological analyasis

Primary tumors and all organs from different injection routes were subjected to histopathological analysis. Tumors and tissues were fixed in 3.7% formaldehyde, 5% glacial acetic acid, and 72% ethanol for at least one day before proceeding to paraffin embedding. Serial 4 μm sections were cut and stained with hematoxylin and eosin for histopathological examinations.

Statistical analysis

Survival analysis was determined by the Kaplan–Meier method, and P-values were assessed by Student's t-test.

Results

Characterizations of HeLa cells with stable and high-level DsRed2 gene expression

To establish DsRed2, red fluorescent protein gene was inserted in the cervical cancer models and to determine the tumorigenic characteristics of HeLa cells resulting from insertional effects, DsRed2-, and neomycin-transduced HeLa cells were selected for resistant cells under 800 μg/ml of neomycin (G418) (Clontech, California, USA). Several high DsRed2-expressing cell clones were selected. These selected HeLa-DsRed2 cells had strikingly intense red fluorescence that remained stable in the absence of selective agents after more than 20 passages as compared to the vector control (Figure 1A). Five clones of HeLa-DsRed2, HeLa-EGFP, HeLa-VC cells were pooled to determine the growth potentials and tumorigenicity *in vitro* and *in vivo*. Figure 1B shows the results of the in vitro growth curves. Even though

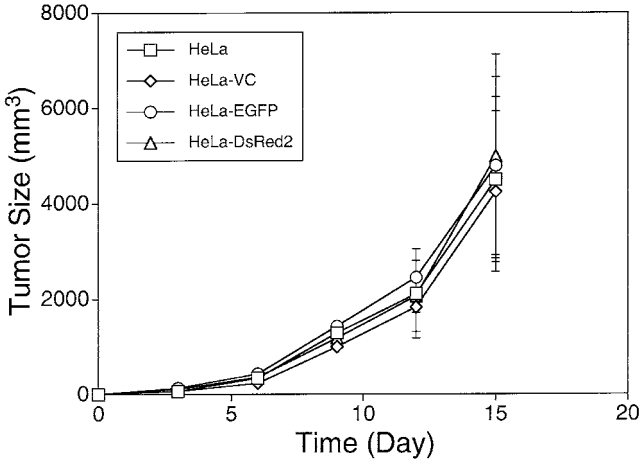

Figure 2. In vivo growth curves of HeLa-DsRed2 and controls. 5×10^6 HeLa, HeLa-VC, Hela-EGFP, or HeLa-DsRed2 cells were injected in the flanks of SCID mice. Since Hela cells induced fast *in vivo* tumor growth, the tumor volumes were recorded once every three days to generate *in vivo* growth curves. Note no statistical differences were noted in HeLa-DsRed2 tumors and controls.

HeLa-DsRed2 cells grew faster than HeLa-EGFP, HeLa-VC, and HeLa cells, there were no statistical differences in the proliferation powers of parental HeLa cells, HeLa-VC, HeLa-EGFP, and HeLa-DsRed2 cells. In addition, colony-forming assay results also showed no statistical differences in HeLa, HeLa-VC, HeLa-EGFP, and HeLa-DsRed2 cells (Figure 1C). The six SCID mice that received subcutaneous injections of 2×10^6 HeLa-DsRed2, HeLa-EGFP, HeLa-VC, or HeLa cells in the flanks were used to determine the *in vivo* tumor growth curves. All of the mice were found with subcutaneous tumors, ranging from 2500 mm^3 to 7500 mm^3 two weeks after injections (Figure 2). There were no statistical differences in tumor volumes of HeLa-DsRed2 (4857 ± 2138 mm^3), HeLa-EGFP (4783 ± 1869 mm^3), HeLa-VC (4239 ± 1682 mm^3), and HeLa (4494 ± 1730 mm^3). Similar to *in vitro* growth curves results, HeLa-DsRed2 cells also grew faster than HeLa-EGFP, HeLa-VC and HeLa cells *in vivo*. However, the differences were not statistically significant. These results show that DsRed2 gene insertions do not interfere with the tumor growth potentials either *in vitro* or *in vivo*.

Subcutaneous HeLa-DsRed2 tumors in SCID mice retained high-level DsRed2 expressions and induced significant lung metastasis

Human cervical carcinomas with systemic metastasis represent the end-stage of the disease. To determine whether HeLa-DsRed2 cells induced metastasis after subcutaneous injections, 5×10^6 HeLa-DsRed2 cells were injected into the left flank of the SCID mice. Two weeks after HeLa-DsRed2 cell injections, most of the mice were found to be moribund. Optical imaging system was applied to visualize red fluorescent tumors or tumor cells in SCID mice. The results showed strong and evenly distributed red fluorescence in the subcutaneous tumors (Figures 3B and D) when compared with their corresponding daylight images (Figures 3A and C). The subcutaneous HeLa-DsRed2 tumor also showed parental epithelial morphology by histopathological analysis (Figures 4A and B). These results show that the existence of red fluorescent protein in HeLa tumor cells remain stable and do not interfere with the tumorigenicity or tumor growth *in vivo*. The mice were further examined for the presence of tumors in different organs. Extensive lung metastasis was observed in these mice (Figures 3E–H, and Table 1). External images showed many fluorescent HeLa-DsRed2 cells in lung parenchyma (Figures 3F and H). Histopathological analysis of the serial sections revealed that most of the HeLa-DsRed2 cells were still at the single-cell level with round morphology in the lungs (Figures 4C and D, white arrowhead). Mild to moderate instances of tumor spread were found in the heart, liver, stomach, spleen, kidney, and ovary. The brain and intestines were not involved (Table 1).

External fluorescence image analysis of HeLa/DsRed2 tumors after intraperitoneal injections

5×10^6 HeLa-DsRed2 cells were injected into SCID mice through the intraperitoneal route. Most of the mice were found to have such clinical symptoms of terminal disease as arched back, rough coat, breathing difficulty, or loss of appetite 14 days after injections. These mice were examined for the presence of HeLa/DsRed2 tumors using fluorescent microscopy. External image analysis showed extensive involvement of tumor foci or tumor cells in the abdominal cavity (Figure 5 and Table 2). Tumor foci were found in liver, kidney, spleen, stomach, and ovary (Figures 5B, D, F, G, and I, respectively). HeLa/DsRed2 tumor cells were also found in peritoneum (Figure 5L). Systemic involvement was found in the lungs at the single-cell level (Figure 5N). Brain involvement was found near blood vessels (Figures 5O–P). Heart involvement was occasionally observed (Table 2). Histopathological analysis of the serial sections showed tumor foci established on the surface of liver, kidney, stomach, and ovary (Figures 6A–H). Tumor cells were found infiltrating into liver parenchyma (Figure 6B, arrowhead, 200×). Single-cell involvement of the HeLa/DsRed2 cells were found in the peritoneum and lung (Figures 6J and L, arrowhead, respectively). These histopathological findings also confirmed the results of the external image analysis by fluorescent microcopy.

External fluorescence image analysis of HeLa-DsRed2 tumors after intravenous injection

Metastasis patterns of HeLa-DsRed2 cells were also evaluated after intravenous injection of 5×10^6 tumor cells into SCID mice. Mice at the terminal stage of disease were sacrificed and evaluated for the presence of HeLa-DsRed2 tumor cells. External image analysis showed numerous tumor foci in the lungs (Figures 7A–F and Table 3), which was confirmed by H&E stain (Figures 8A–B, arrowhead). Brain metastasis at the single-cell level was also detected (Figures 7G–H and Table 3). Tumor cells were found on the surface of the brain (Figure 7H). Histopathological analysis of brain coronal sections also confirmed these findings (Figures 8C–D, arrowhead). No other systemic organs were

Table 1. Metastasis of DsRed2-expressing HeLa cells after subcutaneous implantation in SCID mice.

	Tumor spread								
Mouse #	Brain	Lung	Heart	Liver	Stomach	Intestine	Spleen	Kidney	Ovary
1	–	+++	+	+	–	–	–	–	–
2	–	+++	+	+	–	–	+	+	–
3	–	+++	–	–	–	–	–	–	–
4	–	+++	++	++	+	–	–	+	–
5	–	+++	–	–	–	–	–	–	–
6	–	+++	++	+	–	–	++	+	+
7	–	+++	–	–	–	–	–	–	–
8	–	+++	+	+	+	–	++	+	–
9	–	+++	–	–	–	–	–	–	–
10	–	+++	++	+	–	–	+	+	+

5×10^6 DsRed2-HeLa tumor cells were injected into SCID mice a through subcutaneous route. Animals were sacrificed when moribund and fresh tissues were examined for tumor spread as indicated by DsRed2 expression using inverted fluorescent microscope. + + +: extensive involvement. ++: moderate involvement. +: mild involvement. –: no involvement.

Table 2. Metastasis of DsRed2-expressing HeLa cells after intraperitoneum implantation in SCID mice.

	Tumor spread									
Mouse #	Brain	Lung	Heart	Liver	Stomach	Intestine	Spleen	Kidney	Ovary	Peritoneum
1	–	+	–	+++	+++	++	–	++	++	+
2	–	+	–	++	++	+	++	–	++	–
3	–	+	–	+++	+	++	–	+	+	–
4	+	++	–	+++	++	+++	++	++	++	+
5	+	+	+	+++	+++	+	++	+++	++	+
6	–	+	–	++	++	++	+	++	+	+
7	–	+	–	+++	++	++	–	+	+	–
8	+	+	–	+++	++	+++	++	++	++	+
9	–	+	+	+++	++	++	+	+++	++	+
10	–	+	–	++	+++	++	++	++	++	–

5×10^6 DsRed2-HeLa tumor cells were injected into SCID mice through a intraperitoneal route. Animals were sacrificed when moribund and fresh tissues were examined for tumor spread as inducated by DsRed2 expression using inverted fluorescent microscope. + + +: extensive involvement. ++: moderate involvement. +: mild involvement. –: no involvement.

Table 3. Metastasis of DsRed2-expressing HeLa cells after intravenous implantation in SCID mice.

	Tumor spread								
Mouse #	Brain	Lung	Heart	Liver	Stomach	Intestine	Spleen	Kidney	Ovary
1	+	+++	–	–	–	–	–	–	–
2	–	+++	–	–	–	–	–	–	–
3	+	+++	–	–	–	–	–	–	–
4	–	+++	–	–	–	–	–	–	–
5	–	+++	–	–	–	–	–	–	–
6	–	+++	–	–	–	–	–	–	–
7	+	+++	–	–	–	–	–	–	–
8	–	+++	–	–	–	–	–	–	–
9	–	+++	–	–	–	–	–	–	–
10	–	+++	–	–	–	–	–	–	–

5×10^6 DsRed2-HeLa tumor cells were injected into SCID mice through intravenous route. Animals were sacrificed when moribund and fresh tissues were examined for tumor spread as indicated by DsRed2 expression using inverted fluorescent microscope. + + +: extensive involvement. ++: moderate involvement. +: mild involvement. –: no involvement.

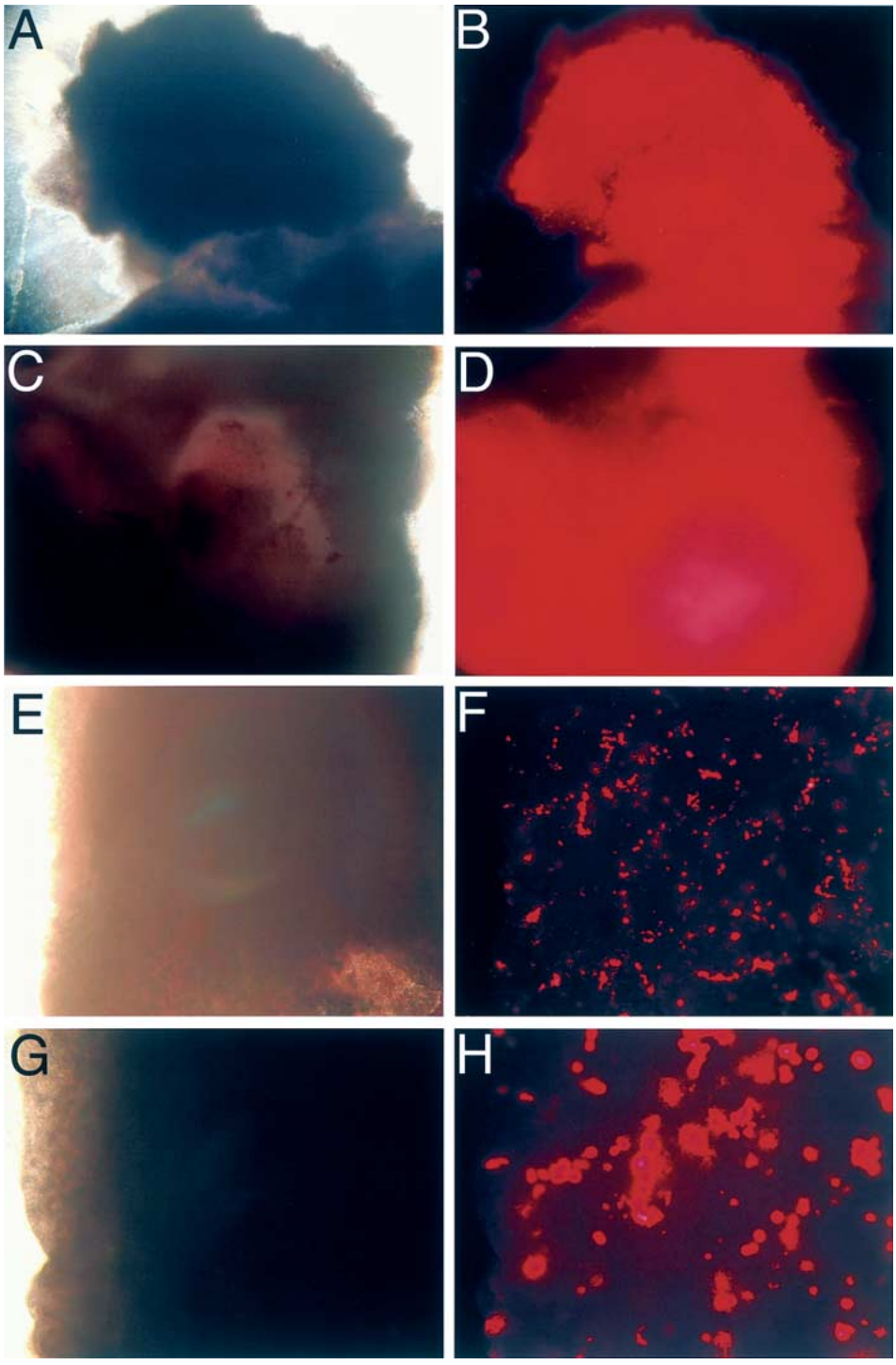

Figure 3. External images of live tumors after subcutaneous injections of HeLa-DsRed2 tumor cells. (A–D) Live HeLa/DsRed2 subcutaneous tumors were excised from the animal and imaged by inverted fluorescent microscopy. (A, C) Daylight pictures of subcutaneous tumors (40×). (B, D) The same subcutaneous tumors observed under a fluorescent microscope with rhodamine filter (40×). (E–H) Detection of HeLa-DsRed2 lung metastasis after subcutaneous injections. (E–F) Daylight and corresponding fluorescent pictures of lung metastasis (40×). (G–H) Daylight and corresponding fluorescent pictures of lung metastasis (200×). Note extensive metastasis with either single cells or small cluster of cells in the lungs.

involved (Table 3). These results showed the lung to be the preferred metastatic site for HeLa-DsRed2 cells after i.v. injections.

To rule out the possibility that lung metatstasis was due to DsRed2 insertional effects, 5×10^6 HeLa-EGFP tumor cells were injected into SCID mice through intravenous route. Similar lung metastatic foci were found in these SCID mice. No statistical differences were found between the numbers and sizes of HeLa-EGFP and HeLa-DsRed2 tumor foci (data not shown).

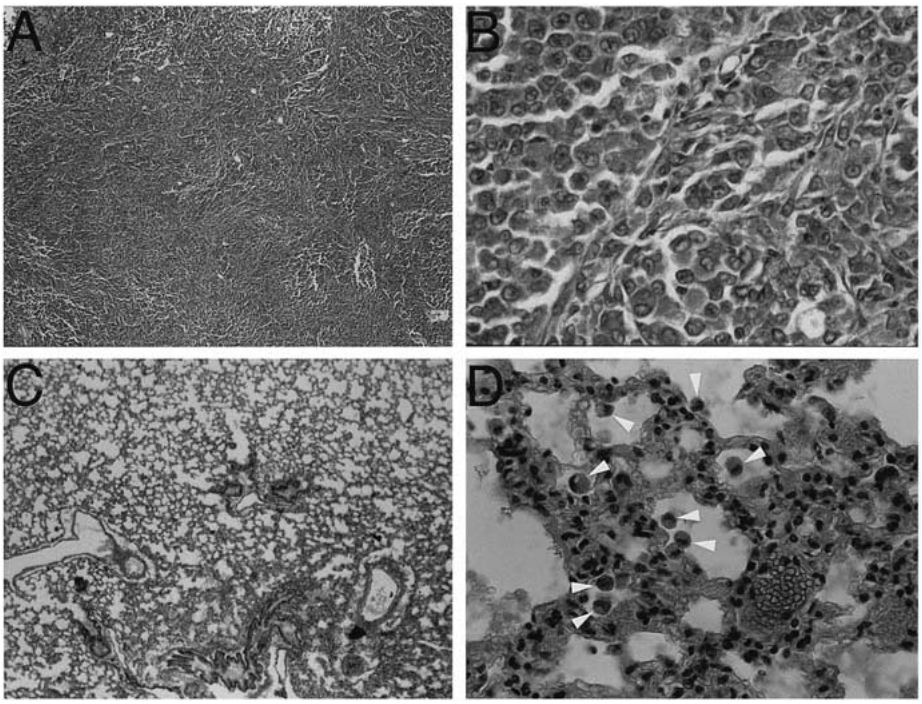

Figure 4. Histopathology of a HeLa-DsRed2 subcutaneous tumor and its lung metastasis. (A–B) Histopathology of HeLa-DsRed2 subcutaneous tumors (H&E stain, (A) 40×, (B) 400×). (C–D) Histopathology of HeLa-DsRed2 lung metastasis (H&E stain, (C) 40×, (D) 400×). White arrowhead showed large round HeLa tumor cells in lung parenchyma.

Comparisons of long-term survival time of SCID mice after receiving subcutaneous, intraperitoneal, or intravenous injection of HeLa-DsRed2 cells

Long-term survival curves were determined to investigate whether implantations of HeLa-DsRed2 tumor cells through different injection route (s.c., i.p., or i.v.) influenced the survival of SCID mice. Emphasis was also placed on the comparison of the survival curves of HeLa-DsRed2 with HeLa-VC to determine whether DsRed2 gene insertion/expression in HeLa cells influenced mean survival time of the SCID mice. Figure 9 showed all of the animals received either subcutaneous or intraperitoneal injections of 5×10^6 HeLa-DsRed2 or HeLa-VC cells died within 16 days after injection. The mean survival time was 11.8 ± 2.3 days after subcutaneous injection and 13.1 ± 1.4 days after intraperitoneal injection of HeLa-DsRed2 cells. A similar mean survival time was found in HeLa-VC injected SCID mice (HeLa-VC-sc, 12.3 ± 2.2 days, and HeLa-VC-ip, 13.6 ± 1.6 days). In comparison, intravenous injections of HeLa-DsRed2 or HeLa-VC tumor cells resulted in statistically significant longer mean survival times of 34.0 ± 6.5 days or 34.2 ± 6.1 days respectively ($P < 0.01$ vs subcutaneous injection, $P < 0.01$ vs intraperitoneal injection). Interestingly, intravenous injection showed more restricted distributions of tumor metastasis (Table 3) as compared to subcutaneous or intraperitoneal injections (Tables 1 and 2). In addition, metastatic foci in lungs were only found after intravenous injections while subcutaneous or intraperitoneal injections induced lung metastasis at the single-cell level. These observations may explain the longer mean survival time of the SCID mice receiving intravenous injections of HeLa-DsRed2 tumor cells.

Discussion

External imaging analysis of internally growing tumors has been performed previously by X-rays, MRI, and ultrasonography. Even though these methods are well suited for the noninvasive imaging of large-scale structures in the human body [27], they have limitations in the investigation of growing tumors at the microscopic level. These conventional optical imaging techniques have also been severely limited by the strong absorbance and scattering of the illuminating light by tissue surrounding the target resulting in insufficient sensitivity and spatial resolution to image early-stage tumor growth or metastasis [28]. In addition, monitoring growth and metastatic dissemination by these methods is impractical because they either use potentially harmful irradiation or require harsh contrast agents and, therefore, cannot be repeated on a frequent, real-time basis. Other attempts such as using labeled monoclonal antibody and other high-affinity vector molecules targeted against tumor- associated markers as specific, detectable spatial markers have mostly met with indifferent success [29–33]. A luciferase gene that emits light has also been developed to monitor spatial temporal gene expression in animals [12, 13]. However, the technique rerquires the transferring of luciferase substrate into mammalian cells. Also, the time duration of the luciferase gene expressions in metastatic tumors has not been determined. Weissleder et al. described a novel approach to the imaging of live tumors [34]. This approach required the infusion

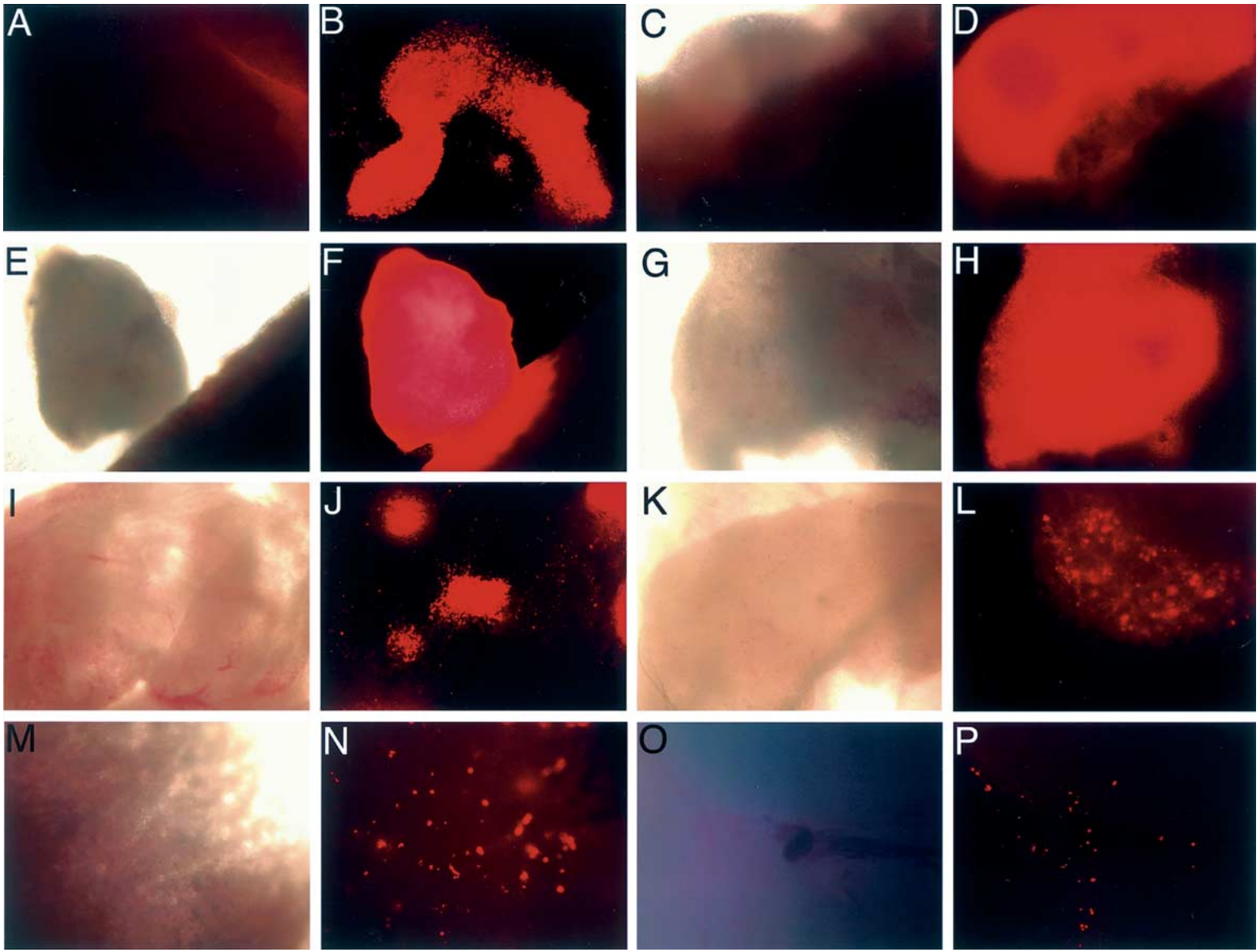

Figure 5. External images of live tumors in multiple organs after intraperitoneal injections of HeLa-DsRed2 tumor cells. (A, C, E, G, I, K, M, O) Daylight pictures of live organs at 40×. (B, D, F, H, J, L, N, P) Pictures of organs under a fluorescent microscope with rhodamine filter (40×). (A–B) Tumor in liver. (C–D) Tumor in kidney. (E–F) Tumor in spleen. (G–H) Tumor in stomach. (I–J) Tumor nodules in ovary. (K–L) Tumor cells localized in peritoneum. (M–N) Lung metastasis. Note moderate involvements with single cell or small cluster of cells. (O–P) Brain metastasis. Note involved tumor cells only found at the single cell level.

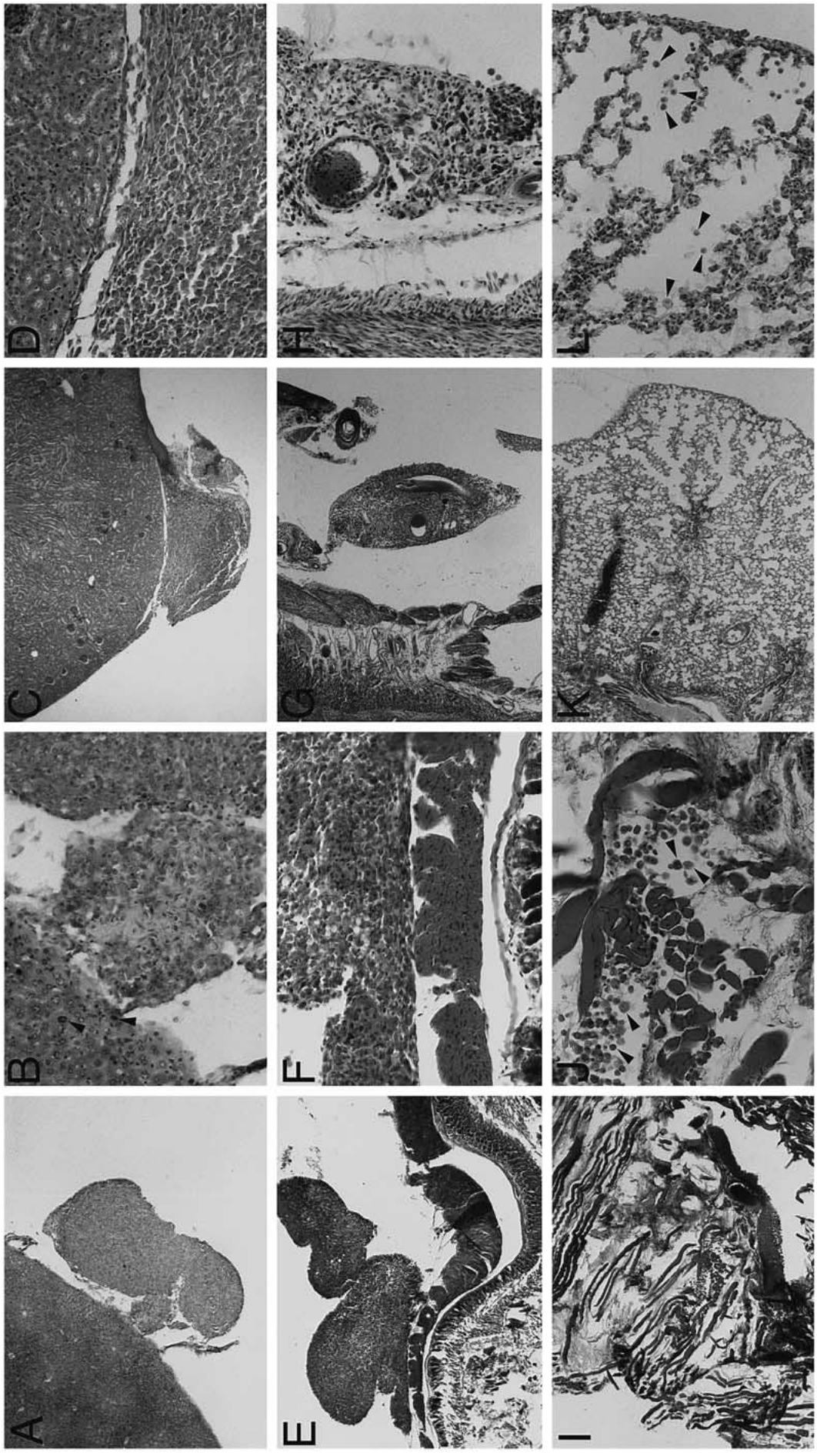

Figure 6. Histopathology of HeLa-DsRed2 tumors in abdominal cavity and their lung metastases. (A–B) Histopathology of HeLa-DsRed2 tumor found in liver ((A) 40×; (B) 200×). Arrowhead showed invasive tumor cells in liver parenchyma. (C–D) Tumor in kidney ((C) 40×; (D) 200×). (E–F) Tumor in stomach ((E) 40×; (F) 200×). (G–H) Tumor in ovary ((G) 40×; (H) 200×). (I–J) Tumor cells in peritoneum ((I) 40×; (J) 200×). Arrowhead represents infiltrating tumor cells in the muscle layer of peritoneum. (K–L) Tumor cell metastasis to lung ((K) 40×; (L) 200< *times*). Arrowhead represented single tumor cells in parenchyma.

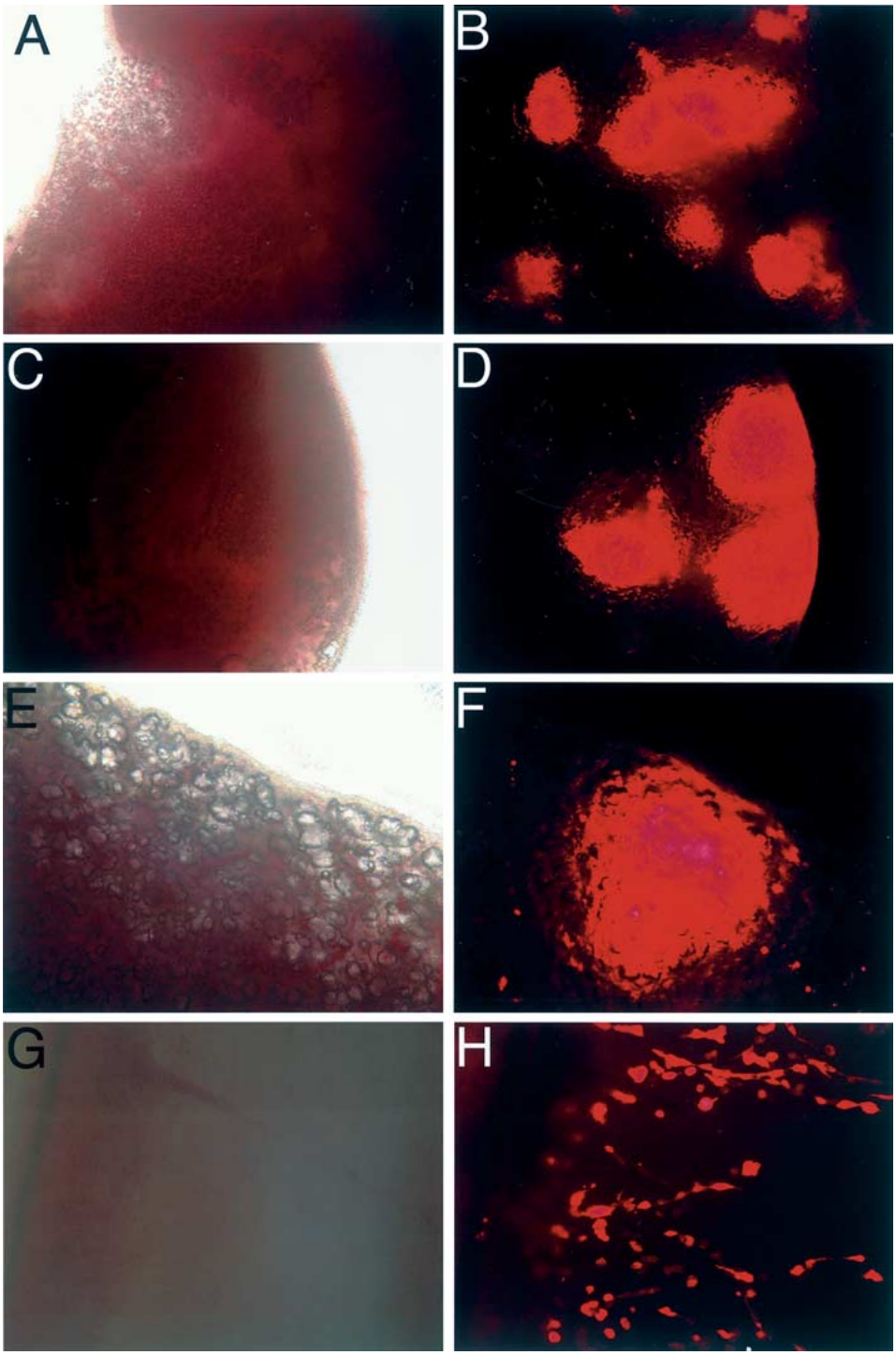

Figure 7. External images of tumor cells in lung and brain after intravenous injections of HeLa-DsRed2 tumor cells. Left panel shows daylight pictures of lung ((A) 40×, (C) 40×, and (E) 200×) and brain ((G) 200×). Right panel shows pictures of lung ((B) 40×, (D) 40×, and (F) 200×) and brain ((H) 200×). Note multiple tumor nodules were found in lung (B, D). Also note single-cell tumor metastasis in brain (H).

of protease-activated, near infra-red fluorescent probes to make the target tissue selectively fluorescent. Tumors with appropriate proteases could activate the probes and be imaged externally. However, most normal tissues also have significant protease activity, a factor that in addition to short half-life of the fluorescence probes, hampers the detection of tumors. The GFP gene/fluorescent microscopy offered an alternative way for the direct and repetitive imaging of tumor growth and metastasis *in vivo*. The GFP expression in cancer cells has been shown to be an effective tumor cell marker over conventional pathological examination procedures, such as histology and immunohistochemistry. In addition, tumor motility, progression, and metastasis can be visualized at single-cell level [17, 19, 34]. The imaging of the GFP-expressing tumor cells requires no preparative procedures and is well suited for visualizing live tissue.

DsRed1, a humanized version of drFP583, has been the subject of extensive research to determine its biochemical

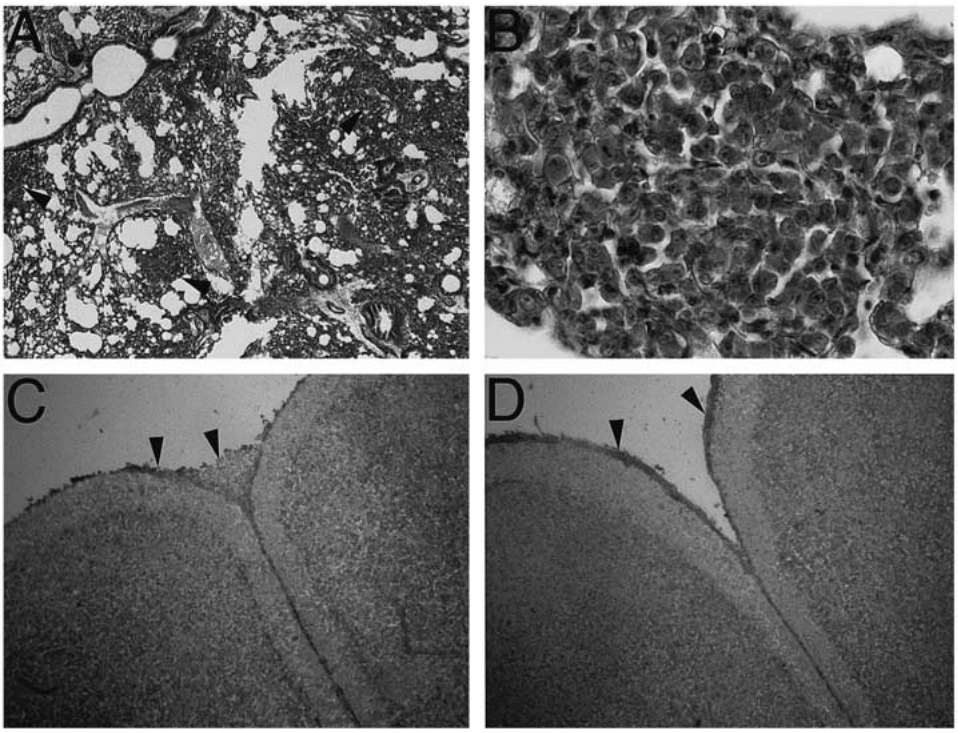

Figure 8. Histopathology of HeLa-DsRed2 tumors in lung and brain after intravenous injections. (A–B) Histopathology of HeLa-DsRed2 tumor nodules in lung ((A) arrowhead, 40×; (B) 400×). (C–D) coronal sections of brain metastasis (40×). Arrowhead shows tumor metastasis from the meningeal surface. (C, D).

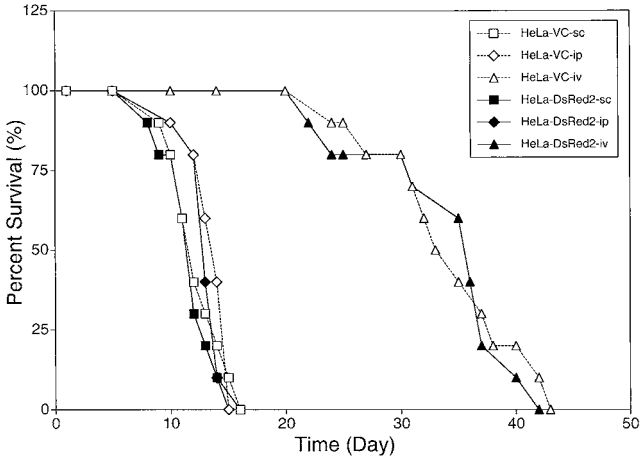

Figure 9. Long-term survival curves of SCID mice after injecting HeLa-DsRed2 through subcutaneous, intraperitoneal, or intravenous route. Ten SCID mice per group were injected with 5×10^6 each of HeLa-Dsred2 cells through subcutaneous, intraperitoneal, or intravenous route. Time of death of the animals was recorded. Percent survival of the animals was calculated to generate long-term survival curves. Note HeLa-DsRed2-ip and HeLa-DsRed2-sc all died within two weeks of injections.

and photophysical properties. DsRed, a 28-kDa polypeptide, has essentially the same chromophore as *av*GFP, autocatalytically formed from an internal Gln-Tyr-Gly (residues 66-68) tripeptide (amino acid sequence numbering of wild-type protein) [21, 35]. The overall amino acid sequence homology to *av*GFP is low, about 23%; however, several amino acids in the immediate vicinity of the chromophore are strictly conserved and are probably essential for chromophore formation (e.g., Glu-215 and Arg-95, corresponding to *av*GFP Glu-222 and Arg-96). The broad excitation and emission bands have maxima at 558 and 583 nm, respectively. An extinction coefficient of 75,000 mol^{-1}/cm^{-1} and a fluorescence quantum yield of 0.7 at the 558-nm excitation wavelength have been reported [22, 23], much higher than the ones initially published by Matz et al. [21]. The protein proves to be stable under harsh pH conditions and is extremely resistant to photobleaching [22]. DsRed is also an excellent fluorescence-resonance energy-transfer counterpart to the yellow fluorescent variants of *av*GFP, which have emission maxima of about 525 nm [36, 37], and its emission is distinct from other forms of GFPs, such as EGFP, ECFP or EYFP, for multi-color detections in flow cytometry [38]. However, two major deficiencies have been discovered: the slow and possibly incomplete maturation for the red fluorescence, which apparently passes through an obligatory green-emitting intermediate similar to avGFP, and its tendency to oligomerize even at dilute concentrations [22, 23, 39]. Yeast two-hybrid assays and cell expression also indicate oligomerization and/or aggregation in living cells [22, 39, 40].

The present study used DsRed2, a new variant of DsRed1, to establish HeLa stable clones. DsRed2 contains six amino acid substitutions: A105V, I116T, S197A, R2A, K5E, and K9T. These mutations improve the solubility of DsRed2 by reducing its tendency to form aggregates and also reduce the time from transfection to detection to only 24 h (data not shown). DsRed2 retains the benefits of a red fluorescent protein, such as a high signal-to-noise ratio and distinct spectral properties for use in multicolor labeling experiments. The DsRed2 signal was also shown to be bright

enough to permit detection from stably introduced transgenes in viable mammalian cells by a fluorescent microscopic methodology. The sustained expression of DsRed2 gene was neither toxic to tumor cells nor inhibiting the growth potentials of HeLa cells (Figures 1B and C). In addition, a rapidly maturing variant of DsRed gene using an asparagine-to-glutamine substitution at position 42 has also been reported [41]. The development of tumor models based on the insertion of a red fluorescent protein gene opens up many new possibilities to experimental design. Most importantly, the tumor cells with different genetic backgrounds can be labeled by at least two different fluorescent colors, allowing for easy determination of chemotherapeutical responses in tumor subpopulations *in vitro* and *in vivo* [42]. In addition, tumors can be labeled in two colors in disparate tumor interference models to allow great flexibility in placement and timing of the tumors, whose growth and angiogenesis can be studied for an unlimited period [24].

The HeLa tumor-metatstasis models were established in this report. Three injection methods including subcutaneous, intraperitoneal, and intravenous were performed. Tumor growth patterns and their pulmonary metastasis were compared. We found extensive pulmonary metastasis with mostly single cell or small clusters of cells in the subcutaneously injected group (Figures 2 and 3). Moderate involvement of single cell pulmonary metastasis was found in the intraperitoneally injected group (Figures 4 and 5). Multiple metastatic nodules were found only in the intravenously injected group (Figures 6 and 7). The patterns of lung metastasis resulting from human cervical carcinomas, multiple pulmonary nodules (71%), mediastinal and hilar lymphadenopathy (32%) and pleural metastases (27%), were frequently observed. Rare findings included bone metastases (6%), endobronchial obstruction (5%), and lymphangitic carcinomatosis (3%). Our results show that the intravenous injected group clearly resemble human pulmonary metastasis of cervical carcinomas. Interestingly, the animals survived less than two weeks after subcutaneous or intraperitoneal injections of HeLa-DsRed2 cells (mean survival time s.c.: 11.8 ± 2.3 days; i.p.: 13.1 ± 1.4 days) whereas the survival time after intravenous injections was longer (mean survival time 34.0 ± 6.5 days). The most likely explanation of the extended survival time in the intravenous-injected group is that most of the tumor cells were trapped in lung parenchyma after the initial injections. A longer time was required for tumor cells to grow as a colony. In contrast, tumor cells seeded to many organs immediately after intraperitoneal injection. Multiple organ failures developed faster and caused the death of the animal. The reason for the faster animal death caused by subcutaneous injection was not clear and remains to be elucidated.

In conclusion, we have used DsRed2 inserted HeLa cervical cancer cells to establish novel metastasis models in SCID mice. We showed extensive distributions of tumor micrometastasis at the single cell level in various major organs such as the lungs, liver, kidney, spleen, stomach, and brain. We further determined the metastatic patterns after s.c., i.p., or i.v. injection of HeLa-DsRed2 cells and confirmed that the i.v. injection method best resembled pulmonary metastasis of human cervical carcinoma. The presence of tumor cells and their invasion/metastasis into organs or tissues can be monitored. The DsRed2 gene insertions into HeLa cells is not toxic to tumor cells and do not alter tumorigenicity *in vitro* on *in vivo*. Our results suggest the feasibility of using the DsRed2 gene to establish a red fluorescent tumor model *in vivo*.

Acknowledgements

We thank Ms Yali Chen for technical assistance. This study was supported by grants from the National Science Council (91-2314-B-182A-167 to H.C.C. and 91-2311-B-075B-001 to M.H.) and Kaohsiung Veterans General Hospital (VGHKS91-45 to J.Y.L., VGHKS91-19, and VGHKS92-53 to M.H.).

References

1. Greenlee RT, Hill-Harmon MB, Murray T et al. Cancer statistics, 2001. CA Cancer J Clin 2001; 51: 15–36.
2. Schoell WM, Janicek MF, Mirhashemi R. Epidemiology and biology of cervical cancer. Semin Surg Oncol 1999; 16: 203–11.
3. Cormio G, Pellegrino A, Landoni F et al. Brain metastases from cervical carcinoma. Tumori 1996; 82: 394–6.
4. Ikeda S, Yamada T, Katsumata N et al. Cerebral metastasis in patients with uterine cervical cancer. Jpn J Clin Oncol 1998; 28: 27–9.
5. Imachi M, Tsukamoto N, Matsuyama T, et al. Pulmonary metastasis from carcinoma of the uterine cervix. Gynecol Oncol 1989; 33: 189–92.
6. Kashimura M, Sugihara K, Toki N et al. The significance of peritoneal cytology in uterine cervix and endometrial cancer. Gynecol Oncol 1997; 67: 285–90.
7. Kim GE, Lee SW, Suh CO et al. Hepatic metastases from carcinoma of the uterine cervix. Gynecol Oncol 1998; 70: 56–60.
8. Shin MS, Shingleton HM, Partridge EE et al. Squamous cell carcinoma of the uterine cervix. Patterns of thoracic metastases. Invest Radiol 1995; 30: 724–9.
9. Shiromizu K, Kasamatsu T, Takahashi M et al. A clinicopathological study of postoperative pulmonary metastasis of uterine cervical carcinomas. J Obstet Gynaecol Res 1999; 25: 245–9.
10. Tellis CJ, Beechler CR. Pulmonary metastasis of carcinoma of the cervix: a retrospective study. Cancer 1982; 49: 1705–9.
11. Wu HS, Yen MS, Lai CR et al. Ovarian metastasis from cervical carcinoma. Int J Gynaecol Obstet 1997; 57: 173–8.
12. Edinger M, Sweeney TJ, Tucker AA et al. Noninvasive assessment of tumor cell proliferation in animal models. Neoplasia 1999; 1: 303–10.
13. Sweeney TJ, Mailander V, Tucker AA et al. Visualizing the kinetics of tumor-cell clearance in living animals. Proc Natl Acad Sci USA 1999; 96: 12044–9.
14. Tewari KS, Taylor JA, Liao SY et al. Development and assessment of a general theory of cervical carcinogenesis utilizing a severe combined immunodeficiency murine- human xenograft model. Gynecol Oncol 2000; 77: 137–48.
15. Chalfie M. Green fluorescent protein. Photochem Photobiol 1995; 62: 651–6.
16. Chalfie M, Tu Y, Euskirchen G et al. Green fluorescent protein as a marker for gene expression. Science 1994; 263: 802–5.
17. Chishima T, Miyagi Y, Wang X et al. Cancer invasion and micrometastasis visualized in live tissue by green fluorescent protein expression. Cancer Res 1997; 57: 2042–7.
18. Hoffman RM. Orthotopic transplant mouse models with green fluorescent protein-expressing cancer cells to visualize metastasis and angiogenesis. Cancer Metastasis Rev 1998; 17: 271–7.

19. Paris S, Chauzy C, Martin-Vandelet N et al. A model of spontaneous lung metastases visualised in fresh host tissue by green fluorescent protein expression. Clin Exp Metastasis 1999; 17: 817–22.
20. Yang M, Baranov E, Jiang P et al. Whole-body optical imaging of green fluorescent protein-expressing tumors and metastases. Proc Natl Acad Sci USA 2000; 97: 1206–11.
21. Matz MV, Fradkov AF, Labas YA et al. Fluorescent proteins from nonbioluminescent Anthozoa species. Nat Biotechnol 1999; 17: 969–73.
22. Baird GS, Zacharias DA, Tsien RY. Biochemistry, mutagenesis, and oligomerization of DsRed, a red fluorescent protein from coral. Proc Natl Acad Sci USA 2000; 97: 11984–9.
23. Gross LA, Baird GS, Hoffman RC et al. The structure of the chromophore within DsRed, a red fluorescent protein from coral. Proc Natl Acad Sci USA 2000; 97: 11990–5.
24. Yang M, Baranov E, Wang JW et al. Direct external imaging of nascent cancer, tumor progression, angiogenesis, and metastasis on internal organs in the fluorescent orthotopic model. Proc Natl Acad Sci USA 2002; 99: 3824–9.
25. Hoffman RM. Green fluorescent protein imaging of tumor cells in mice. Lab Anim. 2002; 31: 34–41.
26. Hsiao M, Tse V, Carmel J et al. Intracavitary liposome-mediated p53 gene transfer into glioblastoma with endogenous wild-type p53 *in vivo* results in tumor suppression and long-term survival. Biochem Biophys Res Commun 1997; 233: 359–64.
27. Tearney GJ, Brezinski ME, Bouma BE et al. *In vivo* endoscopic optical biopsy with optical coherence tomography. Science 1997; 276: 2037–9.
28. Taubes G. Play of light opens a new window into the body. Science 1997; 276: 1991–3.
29. Baum RP, Brummendorf TH. Radioimmunolocalization of primary and metastatic breast cancer. Q J Nucl Med 1998; 42: 33–42.
30. Dessureault S, Koven I, Reilly RM et al. Pre-operative assessment of axillary lymph node status in patients with breast adenocarcinoma using intravenous 99mtechnetium mAb-170H.82 (Tru- Scint AD). Breast Cancer Res Treat 1997; 45: 29–37.
31. Neri D, Carnemolla B, Nissim A et al. Targeting by affinity-matured recombinant antibody fragments of an angiogenesis associated fibronectin isoform. Nat Biotechnol 1997; 15: 1271–5.
32. Pasqualini R, Koivunen E, Ruoslahti E. Alpha v integrins as receptors for tumor targeting by circulating ligands. Nat Biotechnol 1997; 15: 542–6.
33. Teates CD, Parekh JS. New radiopharmaceuticals and new applications in medicine. Curr Probl Diagn Radiol 1993; 22: 229–66.
34. Weissleder R, Tung CH, Mahmood U et al. *In vivo* imaging of tumors with protease-activated near-infrared fluorescent probes. Nat Biotechnol 1999; 17: 375–8.
35. Heikal AA, Hess ST, Baird GS et al. Molecular spectroscopy and dynamics of intrinsically fluorescent proteins: coral red (dsRed) and yellow (Citrine). Proc Natl Acad Sci USA 2000; 97: 11996–2001.
36. Ormo M, Cubitt AB, Kallio K et al. Crystal structure of the Aequorea victoria green fluorescent protein. Science 1996; 273: 1392–5.
37. Wachter RM, Elsliger MA, Kallio K et al. Structural basis of spectral shifts in the yellow-emission variants of green fluorescent protein. Structure 1998; 6: 1267–77.
38. Hawley TS, Telford WG, Ramezani A et al. Four-color flow cytometric detection of retrovirally expressed red, yellow, green, and cyan fluorescent proteins. Biotechniques 2001; 30: 1028–34.
39. Jakobs S, Subramaniam V, Schonle A et al. EFGP and DsRed expressing cultures of *Escherichia coli* imaged by confocal, two-photon and fluorescence lifetime microscopy. FEBS Lett 2000; 479: 131–5.
40. Furuta T, Tomioka R, Taki K et al. *In vivo* transduction of central neurons using recombinant Sindbis virus. Golgi-like labeling of dendrites and axons with membrane-targeted fluorescent proteins. J Histochem Cytochem 2001; 49: 1497–508.
41. Bevis BJ, Glick BS. Rapidly maturing variants of the Discosoma red fluorescent protein (DsRed). Nat Biotechnol 2002; 20: 83–7.
42. Torrance CJ, Agrawal V, Vogelstein B et al. Use of isogenic human cancer cells for high-throughput screening and drug discovery. Nat Biotechnol 2001; 19: 940–5.